

# Optical spectroscopy of faint gigahertz peaked spectrum sources

I.A.G. Snellen<sup>1,2</sup>, R.T. Schilizzi<sup>1,3</sup>, M.N. Bremer<sup>1,6,7</sup>, G.K. Miley<sup>1</sup>, A.G. de Bruyn<sup>4,5</sup>, H.J.A. Röttgering<sup>1</sup>

<sup>1</sup>*Leiden Observatory, P.O. Box 9513, 2300 RA, Leiden, The Netherlands*

<sup>2</sup>*Institute of Astronomy, Madingley Road, Cambridge CB3 0HA, United Kingdom*

<sup>3</sup>*Joint Institute for VLBI in Europe, Postbus 2, 7990 AA, Dwingeloo, The Netherlands*

<sup>4</sup>*Netherlands Foundation for Research in Astronomy, Postbus 2, 7990 AA, Dwingeloo, The Netherlands*

<sup>5</sup>*Kapteyn Institute, Postbus 800, 9700 AV, Groningen, The Netherlands*

<sup>6</sup>*Institut d'Astrophysique de Paris, 98bis Boulevard Arago, 75014 Paris, France*

<sup>7</sup>*Department of Physics, Bristol University, H H Wills Physics Laboratory, Tyndall Avenue, Bristol, BS8 1TL, United Kingdom*

## ABSTRACT

We present spectroscopic observations of a sample of faint Gigahertz Peaked Spectrum (GPS) radio sources drawn from the Westerbork Northern Sky Survey (WENSS). Redshifts have been determined for 19 (40%) of the objects. The optical spectra of the GPS sources identified with low redshift galaxies show deep stellar absorption features. This confirms previous suggestions that their optical light is not significantly contaminated by AGN-related emission, but is dominated by a population of old ( $>9$  Gyr) and metal-rich ( $>0.2$  [Fe/H]) stars, justifying the use of these (probably) young radio sources as probes of galaxy evolution. The optical spectra of GPS sources identified with quasars are indistinguishable from those of flat spectrum quasars, and clearly different from the spectra of Compact Steep Spectrum (CSS) quasars. The redshift distribution of the GPS quasars in our radio-faint sample is comparable to that of the bright samples presented in the literature, peaking at  $z \sim 2 - 3$ . It is unlikely that a significant population of low redshift GPS quasars is missed due to selection effects in our sample. We therefore claim that there is a genuine difference between the redshift distributions of GPS galaxies and quasars, which, because it is present in both the radio-faint and bright samples, can not be due to a redshift-luminosity degeneracy. It is therefore unlikely that the GPS quasars and galaxies are unified by orientation, unless the quasar opening angle is a strong function of redshift. We suggest that the GPS quasars and galaxies are unrelated populations and just happen to have identical observed radio-spectral properties, and hypothesise that GPS quasars are a sub-class of flat spectrum quasars.

## 1 INTRODUCTION

Gigahertz Peaked Spectrum (GPS) sources are a class of compact radio source, characterised by a convex radio spectrum peaking at a frequency of  $\sim 1$  GHz. Together with the class of Compact Steep Spectrum (CSS) sources, which have spectra peaking at lower frequencies, they form a significant fraction ( $\sim 30\%$ ) of the high frequency radio source population (see O’Dea 1998, for a recent review on GPS and CSS sources). Their optical counterparts are a mixture of quasars and galaxies, with the quasars preferentially found at significantly higher redshifts than the galaxies ( $z \sim 2 - 3$ , O’Dea et al 1991, Stanghellini et al. 1998). The VLBI-morphologies (Stanghellini et al. 1997) and the distributions of radio spectral peak frequencies (de Vries et al., 1997; Snellen et al., 1998b) also seem to be different for GPS galaxies and quasars. These differences cause severe

problems for orientation-based unification of GPS galaxies and quasars.

Their small sizes ( $\sim 100$  pc) have made GPS sources the prime candidate to represent the early stages of radio source evolution (Fanti et al. 1995, Readhead et al. 1996, O’Dea and Baum 1997). The alternative hypothesis, which assumes these sources to be small due to confinement by a particularly dense interstellar medium (O’Dea et al. 1991), is less likely as recent observations show that the surrounding media of GPS sources are not significantly different from large scale sources (eg. Fanti et al. 1995). In addition, Owsianik and Conway (1998) have determined that the dynamical age of the radio source 0710+319, a prototype GPS galaxy, to be  $\sim 10^3$  years by measuring the propagation velocity of its hot spots. It is therefore likely that at least some of the GPS galaxies represent the young counterparts of “old” extended radio sources. These are therefore the objects of choice to study the initial evolution of radio sources. Investigating the

optical hosts and environments of GPS sources provides important information on the circumstances under which a radio source is formed.

Here we present results on a sample of faint GPS sources (Snellen 1997) selected from the Westerbork Northern Sky Survey (WENSS; Rengelink et al. 1997). The combination of this new faint sample and existing brighter samples (Fanti et al 1990; O’Dea et al 1991; Stanghellini et al., 1998; de Vries et al., 1997) allow for the first time the disentanglement of redshift and radio luminosity effects.

Previous papers have described the selection (Snellen et al. 1998a), and optical and near-infrared imaging of the radio-faint GPS sample (Snellen et al. 1998b). This paper describes the spectroscopic observations, leading to a discussion of the emission and absorption line properties and the redshift distributions of the GPS galaxies and quasars.

## 2 THE SAMPLE

The selection of the sample has been described in detail in Snellen et al. (1998a). Candidate GPS sources selected from the Westerbork Northern Sky survey, are those with an inverted spectrum between 325 MHz and higher frequencies. The sources are located in two regions of the survey; one at  $15^h < \alpha < 20^h$  and  $58^\circ < \delta < 75^\circ$ , which is called the *mini-survey* region (Rengelink et al. 1997), and the other at  $4^h00^m < \alpha < 8^h30^m$  and  $58^\circ < \delta < 75^\circ$ . Additional observations at 1.4, 5, 8.4 and 15 GHz were carried out with the WSRT and the VLA, yielding a sample of 47 genuine GPS sources with peak frequencies ranging from 500 MHz to more than 15 GHz, and peak flux densities ranging from  $\sim 30$  to  $\sim 900$  mJy. This sample has been imaged in the optical and near-infrared, resulting in an identification fraction of  $\sim 87\%$  (Snellen et al. 1998b).

The subsample for which we obtained optical spectra was selected in the following way. During the first observing session with the William Herschel Telescope (WHT), 5 of the 15 GPS sources in the mini-survey region identified with  $R > 22$  GPS objects were observed, but no redshifts could be determined due to the low signal-to-noise ratio of these observations. Subsequently, we concentrated on the brighter sources in the sample. In the mini-survey region the 11 sources identified with an  $R < 22.0$  object were observed. In the region between  $4^h00^m < R.A. < 8^h30^m$ , the eight sources identified with an  $R < 20.0$  object were observed, except for B0441+5757 which could not be observed due to scheduling constraints.

## 3 OBSERVATIONS AND REDUCTION

The observations were carried out using the 2.5m Isaac Newton Telescope (INT) and the 4.2m William Herschel telescope (WHT). Some of these observations were done as part of a programme carried out in the international CCI observing period on the La Palma telescopes in 1995. Table 1 gives the log of the observations. The ISIS long slit spectrograph was used for the WHT observations, with a  $1024 \times 1024$  Tektronix CCDs in both the red and blue arms. A spectral resolution of  $\sim 15\text{\AA}$  was obtained between 3500 and 9000

**Table 1.** Log of the Observations. Column 1 gives the source-name, column 2 the  $R$  band magnitude from Snellen et al. (1998b), column 3 the telescope used, column 4 the date of observations, and column 5 the exposure time.

Object	$m_R$ (mag)	Tel.	Date	Exp. (sec)
B0531+6121	19.0	WHT	20 Dec. 1995	1800
B0537+6444	19.5	WHT	8 Jan. 1997	1800
B0544+5847	19.4	WHT	8 Jan. 1997	1800
B0601+5753	19.1	WHT	20 Dec. 1995	1800
B0755+6354	19.1	WHT	20 Dec. 1995	1800
B0758+5929	19.3	WHT	8 Jan. 1997	1800
B0826+7045	19.7	WHT	8 Jan. 1997	1800
B0830+5813	15.9	INT	11 Nov. 1996	600
B1525+6801	23.1	WHT	25 Jul. 1995	3000
B1538+5920	20.9	WHT	20 Jun. 1997	1800
B1550+5815	16.7	INT	30 Jul. 1995	1200
B1551+6822	23.8	WHT	26 Jul. 1995	3000
B1557+6220	22.5	WHT	24 Jul. 1995	3000
B1622+6630	17.2	WHT	12 Aug. 1996	3000
B1642+6701	17.0	INT	30 Jul. 1995	1200
B1647+6225	22.9	WHT	12 Aug. 1996	3000
B1746+6921	19.2	INT	30 Jul. 1995	1800
B1819+6707	17.7	INT	30 Jul. 1995	2400
B1841+6715	20.5	WHT	31 Aug. 1994	3600
B1942+7214	23.0	WHT	26 Jul. 1995	3000
B1945+6024	20.4	INT	30 Jul. 1995	3000
B1946+7048	16.3	INT	30 Jul. 1995	900
B1954+6146	22.2	WHT	25 Jul. 1995	3000
B1958+6158	19.1	WHT	19 Jun. 1997	1800

$\text{\AA}$ , using a slit width of  $2''$  and R158 gratings. The Intermediate Dispersion Spectrograph (IDS) was used for the INT observations, with a Tektronix CCD. A spectral resolution of  $\sim 10\text{\AA}$  was obtained between 4000 and 7500  $\text{\AA}$  using a slit width of two arcsec and a grating with 300 grooves/mm. Usually the slit was oriented near the parabolic angle.

The reduction of the spectra was carried out using the ‘Long Slit’ package of the NOAO’s IRAF reduction software. A bias frame was constructed by averaging ‘zero second’ exposures taken at the beginning of each night. This was subtracted from every non-bias frame. The pixel-to-pixel variations were calibrated using flat fields obtained from an internal quartz lamp. Wavelength calibration was carried out by measuring the positions on the frames of known lines from either an Cu-Ne or a Cu-Ar calibration lamp. The sky contribution was removed by subtracting a sky spectrum obtained by fitting a polynomial to the intensities measured along the spatial direction outside the vicinity of targets. One dimensional spectra were extracted by averaging in the spatial direction over an aperture as large as the spatial extent of the brightest emission line.

## 4 RESULTS

Redshifts were determined for all 11 sources in the mini-survey region identified with an  $R < 22.0$  object, and for 8 sources in the region between  $4^h00^m < R.A. < 8^h30^m$ , which are all sources in this region identified with an  $R < 20.0$  object, except B0441+5757. Five of the 15 GPS sources

**Table 2.** Emission line properties of GPS sources. column 1 gives the source name, column 2 the identification (Q/G), column 3 the observed wavelengths of the emission lines, column 4 the redshifts, column 5 the line flux, column 6 the FWHM, and column 7 the rest-frame equivalent width.

Object	ID	Line	Peak Å	Redshift	Flux $10^{-16} \frac{erg}{cm^2 s}$	FWHM km/s	Eq. Width (rest) Å
B0531+6121	G	[OII]	5266.9 ± 0.9	0.414 ± 0.0010			
		Hβ	6875.5 ± 0.6	0.413 ± 0.0002	24.2 ± 2.4	< 382	50 ± 6
		[OIII]	7016.1 ± 0.6	0.414 ± 0.0001	12.4 ± 1.4	< 349	15 ± 2
		[OIII]	7016.1 ± 0.6	0.415 ± 0.0001	48.5 ± 8.0	< 285	44 ± 5
		[OIII]	7084.1 ± 0.5	0.415 ± 0.0001	128.3 ± 14.4	604 ± 280	160 ± 16
B0537+6444	Q	Lyα	4154.6 ± 1.2	2.417 ± 0.0010			
		SiIV/O	4782.6 ± 31.1	2.417 ± 0.0010	44.2 ± 6.0	2550 ± 250	159 ± 16
		CIV	5292.8 ± 1.8	2.416 ± 0.0222	3.0 ± 1.0	3580 ± 700	10 ± 2
		CIV	5292.8 ± 1.8	2.417 ± 0.0012	17.3 ± 2.7	2800 ± 300	50 ± 5
		CIII]	6509.7 ± 7.7	2.410 ± 0.0040	8.6 ± 1.2	2150 ± 200	23 ± 2
B0544+5847	Q		2.860 ± 0.0070				
		Lyα	4780.5 ± 151.9	2.931 ± 0.1250	15.0 ± 2.3	13500 ± 1500	17 ± 2
		CIV	5977.5 ± 10.8	2.859 ± 0.0070	4.5 ± 0.9	5350 ± 1000	7 ± 1
		CIII]	7350.0 ± 26.9	2.850 ± 0.0141	4.0 ± 0.8	3300 ± 600	7 ± 1
B0601+5753	Q			1.840 ± 0.0020			
		CIV	4402.5 ± 3.8	1.842 ± 0.0025	30.0 ± 5.8	3650 ± 400	42 ± 4
		HeII	4652.8 ± 4.7	1.837 ± 0.0029	3.0 ± 0.7	1450 ± 300	6 ± 1
		CIII]	5425.0 ± 10.5	1.842 ± 0.0055	4.5 ± 1.1	2650 ± 500	10 ± 2
		MgII	7992.6 ± 59.8	1.856 ± 0.0212	7.4 ± 2.0	4850 ± 900	26 ± 3
B0755+6354	Q	Lyα	4872.7 ± 1.3	3.005 ± 0.0010			
		CIV	6194.4 ± 2.6	3.007 ± 0.0011	148.2 ± 14	1750 ± 200	110 ± 9
		CIV	6194.4 ± 2.6	2.999 ± 0.0017	53.3 ± 5.3	3600 ± 350	57 ± 6
B0758+5929	Q	CIV	4612.2 ± 29.8	1.977 ± 0.0190	8.9 ± 0.9	6400 ± 650	25 ± 3
		CIII]	5652.7 ± 179.5	1.978 ± 0.0193	5.1 ± 0.5	9350 ± 1000	14 ± 2
		CIII]	5652.7 ± 179.5	1.961 ± 0.0946	5.1 ± 0.5	9350 ± 1000	14 ± 2
B0826+7045	Q	SiIV/O	4204.5 ± 87.4	2.003 ± 0.0010			
		CIV	4659.7 ± 6.9	2.003 ± 0.0624	8.5 ± 0.8	7950 ± 1800	18 ± 5
		HeII	4919.3 ± 2.5	2.008 ± 0.0044	39.9 ± 4.0	6150 ± 600	42 ± 5
		HeII	4919.3 ± 2.5	2.000 ± 0.0015	3.6 ± 0.4	— <sup>a</sup>	4 ± 1
		CIII]	5720.6 ± 2.1	2.000 ± 0.0015	3.6 ± 0.4	— <sup>a</sup>	4 ± 1
B0830+5813	G	NII	7188.3 ± 4.3	0.093 ± 0.0007 <sup>b</sup>	16.2 ± 1.6	1796 ± 434	15 ± 2
		NII	7188.3 ± 4.3	0.093 ± 0.0007	16.2 ± 1.6	1796 ± 434	15 ± 2
B1538+5920	Q	Lyα	5929.2 ± 1.2	3.878 ± 0.0010			
		NV	6054.6 ± 1.6	3.876 ± 0.0009	11.2 ± 0.8	1900 ± 200	37 ± 4
		CIV	7544.2 ± 3.9	3.883 ± 0.0013	3.4 ± 0.3	2700 ± 270	13 ± 1
		CIV	7544.2 ± 3.9	3.870 ± 0.0025	9.7 ± 0.4	2500 ± 250	35 ± 10
B1550+5815	Q	CIII]	4427.7 ± 5.3	1.324 ± 0.0020			
		MgII	6509.0 ± 5.2	1.319 ± 0.0028	395.1 ± 40	4550 ± 500	20 ± 2
		MgII	6509.0 ± 5.2	1.325 ± 0.0019	320.7 ± 32	3300 ± 350	31 ± 3
B1622+6630	G			0.201 ± 0.0003			
		[OII]	4490.9 ± 2.0	0.205 ± 0.0015	7.3 ± 1.1	< 400	18 ± 3
		Hβ	5835.4 ± 0.8	0.200 ± 0.0002	4.6 ± 0.5	< 267	6 ± 1
		[OIII]	5958.8 ± 0.8	0.202 ± 0.0002	21.1 ± 2.2	< 300	10 ± 2
		[OIII]	6016.6 ± 0.8	0.202 ± 0.0002	51.7 ± 5.2	< 330	25 ± 3
		Hα	7895.2 ± 2.9	0.203 ± 0.0004	312.0 ± 31.5	3540 ± 347	114 ± 12
B1642+6701	Q	SiIV/O	4055.4 ± 2.4	1.895 ± 0.0010			
		CIV	4484.0 ± 1.6	1.897 ± 0.0017	158.0 ± 16	5550 ± 1100	7 ± 1
		CIV	4484.0 ± 1.6	1.895 ± 0.0010	469.0 ± 64	6000 ± 600	27 ± 3
		CIII]	5505.9 ± 20.1	1.884 ± 0.0105	263.0 ± 26	5300 ± 500	21 ± 2
B1647+6225	Q	Lyα	3869.7 ± 2.0	2.167 ± 0.0010			
		NV	3942.4 ± 5.7	2.182 ± 0.0019	9.8 ± 1.0	2850 ± 300	181 ± 18
		CIV	4926.3 ± 1.9	2.179 ± 0.0046	3.5 ± 0.4	3400 ± 350	69 ± 7
		CIV	4926.3 ± 1.9	2.180 ± 0.0012	4.3 ± 0.4	2700 ± 300	126 ± 25
		CIII]	6063.9 ± 7.6	2.176 ± 0.0044	1.1 ± 0.2	2200 ± 250	32 ± 3

<sup>a</sup> No reliable determination of FWHM possible due to associated absorption.

<sup>b</sup> several stellar absorption lines are present consistent with the emission line redshift.

Object	ID	Line	Peak Å	Redshift	Flux $10^{-16} \frac{\text{erg}}{\text{cm}^2 \text{s}}$	FWHM km/s	Eq. Width (rest) Å
B1746+6921	Q	CIV	$4468.9 \pm 8.4$	$1.886 \pm 0.0040$	$20.8 \pm 2.1$	$2500 \pm 500$	$9 \pm 1$
		CIII]	$5514.4 \pm 14.4$	$1.889 \pm 0.0075$	$32.0 \pm 3.2$	$5650 \pm 550$	$17 \pm 2$
B1819+6707	G	[OII]	$4546.6 \pm 1.2$	$0.220 \pm 0.0003$	$5.7 \pm 0.7$	< 442	$22 \pm 3$
		[OIII]	$6047.1 \pm 4.8$	$0.219 \pm 0.0010$	$2.2 \pm 0.4$	< 615	$3 \pm 1$
		[OIII]	$6110.2 \pm 1.8$	$0.220 \pm 0.0004$	$4.6 \pm 0.6$	< 372	$6 \pm 2$
B1841+6715	G	[OII]	$5459.1 \pm 1.1$	$0.470 \pm 0.0100$	$1.9 \pm 0.3$	< 366	$13 \pm 2$
		H $\beta$	$7220.8 \pm 2.0$	$0.485 \pm 0.0004$	$0.4 \pm 0.1$	< 300	$2 \pm 1$
		[OIII]	$7433.3 \pm 1.9$	$0.485 \pm 0.0004$	$3.9 \pm 0.5$	$317 \pm 305$	$23 \pm 2$
B1945+6024	Q	Ly $\alpha$	$4519.0 \pm 13.0$	$2.700 \pm 0.0080$	$3.3 \pm 0.3$	$7150 \pm 1400$	$12 \pm 2$
		CIV	$5724.6 \pm 8.1$	$2.716 \pm 0.0106$	$1.9 \pm 0.2$	$3900 \pm 800$	$7 \pm 1$
B1946+7048	G	[OII]	$4107.3 \pm 1.3$	$0.101 \pm 0.0005$	$7.6 \pm 2.3$	< 503	$24 \pm 3$
		H $\beta$	$5353.7 \pm 1.3$	$0.102 \pm 0.0003$	$5.4 \pm 0.8$	< 388	$4 \pm 0$
		[OIII]	$5460.1 \pm 2.6$	$0.101 \pm 0.0005$	$4.0 \pm 1.5$	< 400	$3 \pm 1$
		[OIII]	$5514.4 \pm 1.2$	$0.101 \pm 0.0002$	$9.2 \pm 1.5$	< 366	$7 \pm 1$
		[OI]	$6935.4 \pm 2.0$	$0.101 \pm 0.0003$	$8.0 \pm 1.1$	< 306	$5 \pm 1$
B1958+6158	Q	Ly $\alpha$	$4628.5 \pm 1.3$	$1.824 \pm 0.0010$	$106.0 \pm 15$	$3350 \pm 350$	$81 \pm 8$
		SiIV/O	$3952.8 \pm 6.9$	$1.823 \pm 0.0008$	$23.0 \pm 3.0$	$5500 \pm 550$	$18 \pm 1$
		CIV	$4373.8 \pm 1.5$	$1.823 \pm 0.0049$	$57.0 \pm 7.0$	$2650 \pm 300$	$37 \pm 4$
		HeII	$4629.5 \pm 1.6$	$1.824 \pm 0.0009$	$4.0 \pm 0.6$	$2200 \pm 500$	$3 \pm 1$
		CIII]	$5382.4 \pm 8.3$	$1.823 \pm 0.0010$	$4.0 \pm 0.6$	$2200 \pm 500$	$3 \pm 1$
		MgII	$5382.4 \pm 8.3$	$1.819 \pm 0.0043$	$18.0 \pm 2.4$	$5650 \pm 550$	$17 \pm 2$
			$7907.8 \pm 2.6$	$1.825 \pm 0.0009$	$9.0 \pm 1.4$	$1400 \pm 300$	$11 \pm 2$

Table 2. Continued...

in the mini-survey region identified with  $R > 22$  GPS objects were observed, but no redshifts could be determined: For four objects no lines were seen at a level of  $> 2 \times 10^{16}$  and the signal-to-noise ratio was too poor to detect absorption against the faint continuum. In addition, there were no spectral features observed in B1954+6154 to determine the redshift (see below). The spectra of the 19 sources with determined redshifts and of B1954+6154 are shown in figure 1. Their emission line properties are given in table 2. The final redshifts of the objects and their uncertainties were determined, taking into account the redshift differences and uncertainties of the individual lines. A distinction between galaxies and quasars has been made on grounds of optical morphology (stellar-extended) and emission line widths. A distinction between galaxies and quasars has been made on grounds of optical morphology (stellar-extended) and emission line widths. The optical host is called a quasar when there is no resolved galaxy visible in the optical CCD-image (Snellen et al. 1998b) and the spectrum shows emission lines with FWHM  $> 2500 \text{ km sec}^{-1}$ .

One of the objects, B1954+6146, has a very peculiar spectrum. Below  $6000 \text{ \AA}$ , the spectrum is faint and flat, while redward of  $6000 \text{ \AA}$  a steep rise in luminosity occurs. It was therefore not clear whether we should classify this object as a galaxy or a quasar. No lines could be identified. The  $R$  band image of this object (Snellen et al. 1998b) shows a point source surrounded by faint extended emission. It is likely that the optical morphology and spectrum are produced by a non-thermal quasar nucleus visible in the red, but obscured in the blue. This would imply a reddening of about 9-10 magnitudes in the  $R$  band, assuming a

flat spectral energy distribution for the quasar nucleus and a standard  $1/\lambda$  extinction curve.

#### 4.1 The Optical Spectra of GPS Galaxies

We obtained reliable spectra for six GPS galaxies, namely B0531+6121, B0830+5813, BG1622+6630, B1819+6707, B1841+6715 and B1946+7048. The spectra of two of the galaxies are clearly dominated by light coming from the active nucleus: B0531+6121 has a powerlaw spectrum and can be classified as a narrow-line radio galaxy with bright Seyfert 2-like emission lines. B1622+6630 can be classified as a Seyfert 1.5 with broad (FWHM  $\sim 3500 \text{ km/s}$ ) H $\alpha$  emission, and resembles the well known GPS galaxy B1404+286 (OQ208, MrK668, eg. O’Dea et al. 1991, and references therein). The broadline region of B1622+6630 seems to be heavily obscured and only visible in the red part of the spectrum. Unlike in B0531+6121, stellar absorption line features and the  $4000 \text{ \AA}$  break are visible in the blue part of the spectrum of B1622+6630 indicating that the non-stellar nuclear light is less prominent in the blue. The emission lines of the other four GPS galaxies are typical for radio galaxies, showing [OII]  $\lambda 3727$ , the [OIII]  $\lambda 4959$  and  $\lambda 5007$  lines, H $\alpha$ /NII, H $\beta$  and in one case (B1946+7048) [OI]  $\lambda 6300$ . Their [OII]/[OIII] line ratios indicate low ionisation.

The optical to near-infrared broadband colours and magnitudes are consistent with GPS galaxies being giant elliptical galaxies with old stellar populations (Snellen et al., 1996a,b.; O’Dea et al. 1996). The spectra obtained here can be used to determine whether the properties of the stellar absorption lines are consistent with this hypothesis. Stellar absorption lines are a more powerful tool than broadband

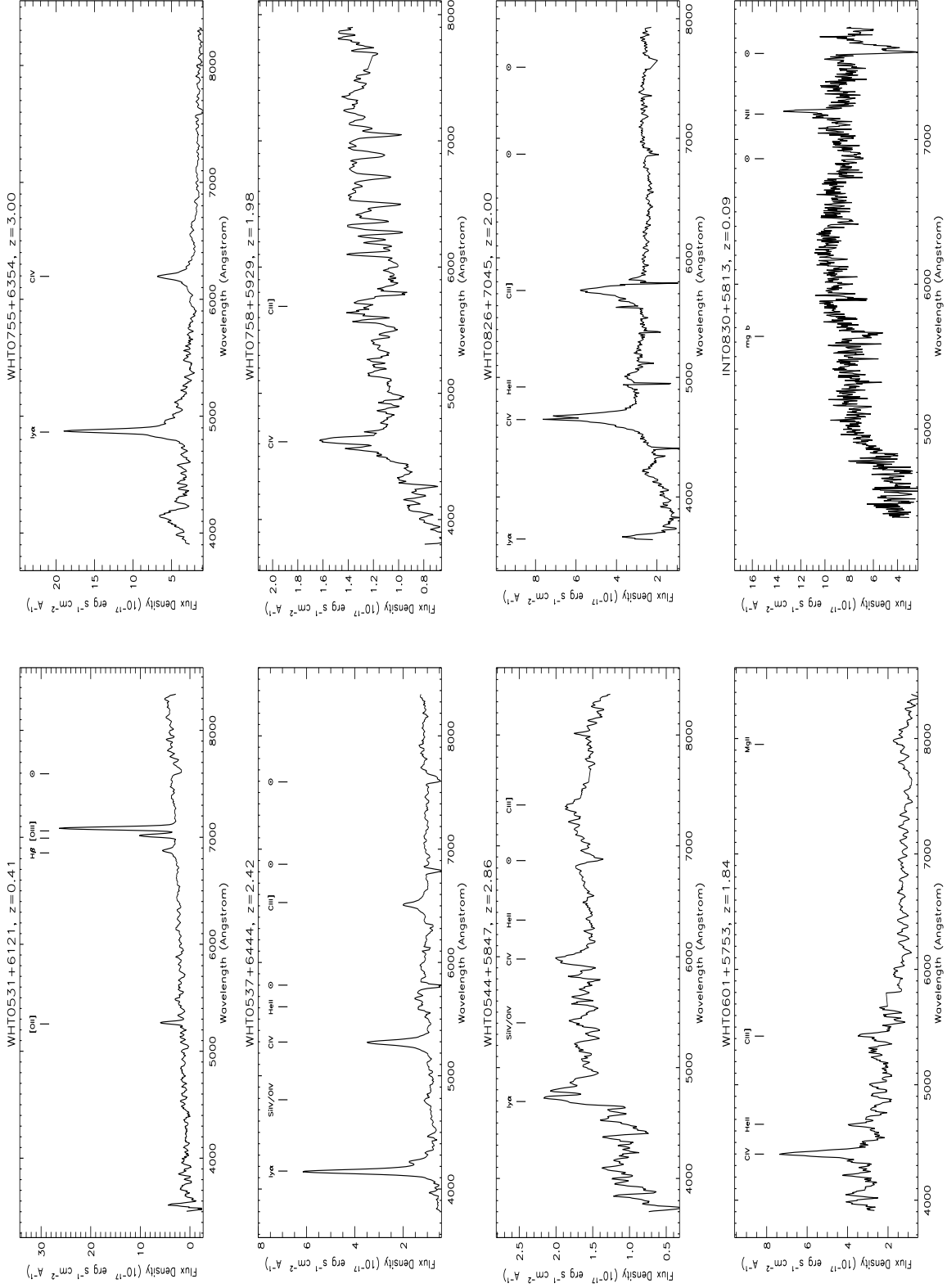


Figure 1. The optical spectra.

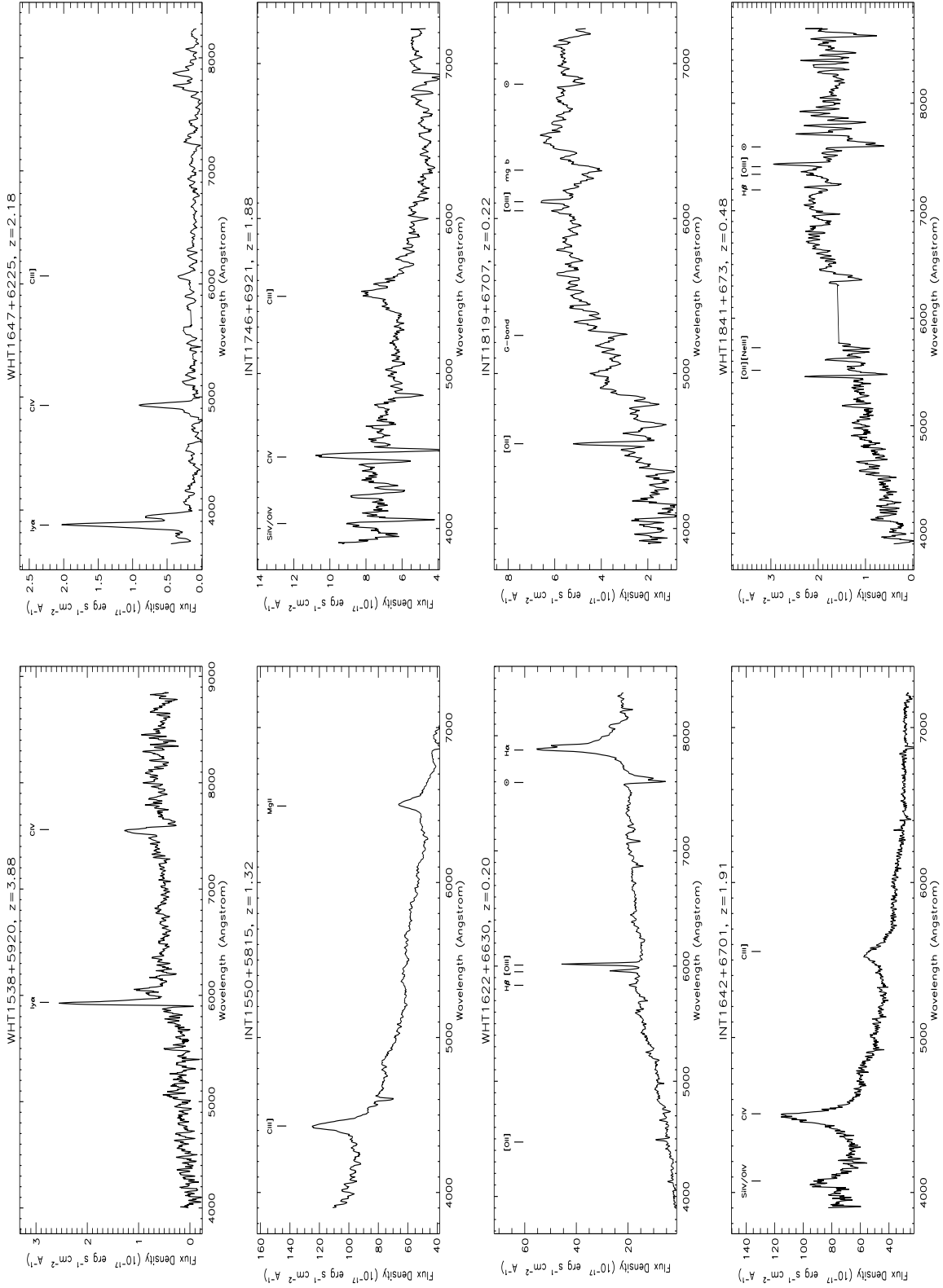


Figure 1. Continued...

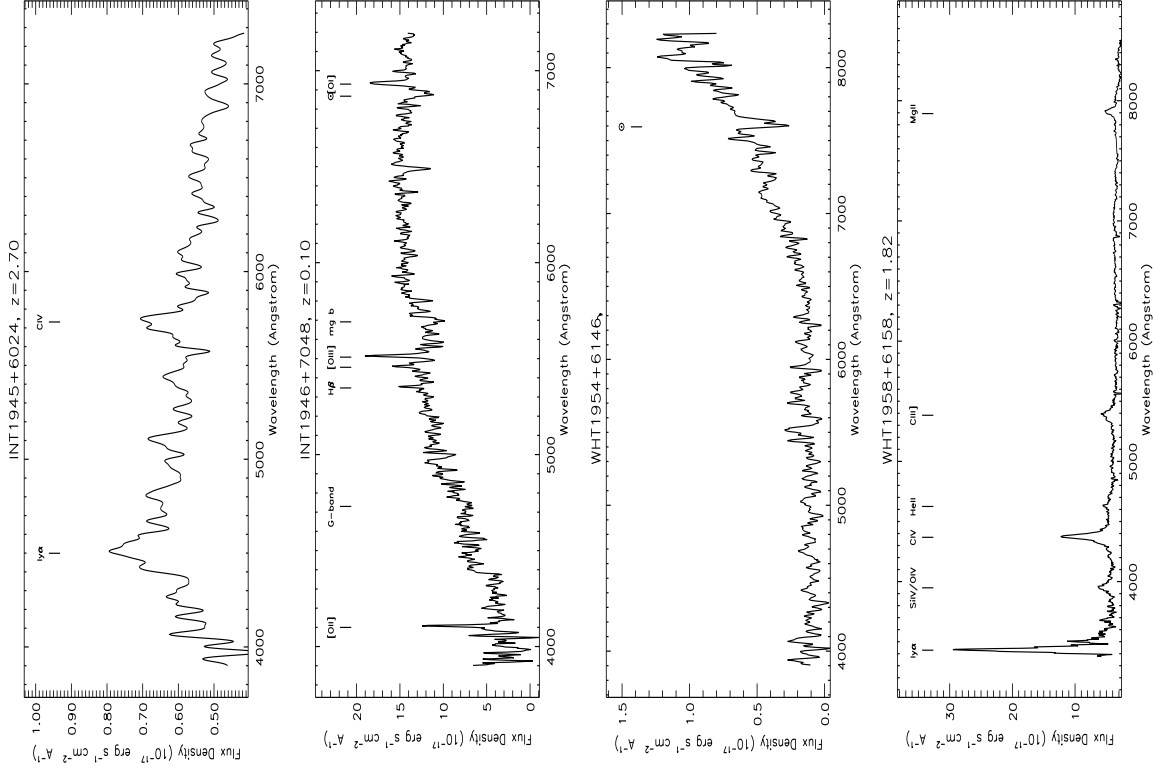
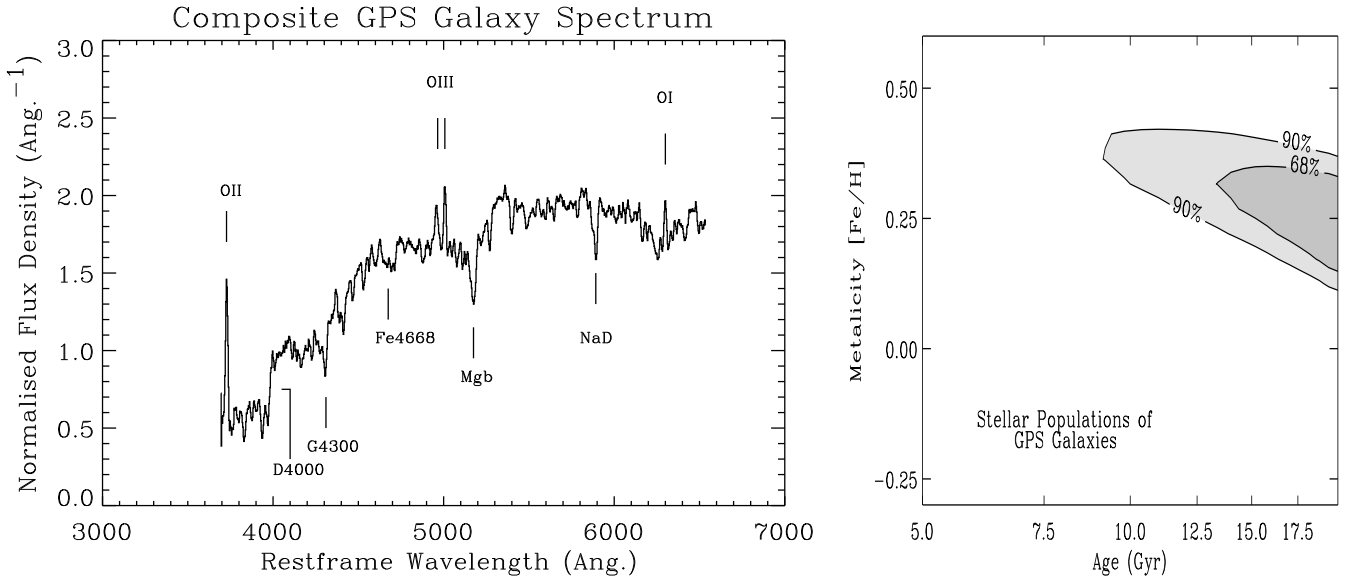


Figure 1. Continued...



**Figure 2.** (left) Composite GPS galaxy spectrum constructed from the three low redshift galaxies in our sample (B0830+5813 at  $z=0.09$ , B1819+6707 at  $z=0.22$ , and B1946+7048 at  $z=0.10$ ). Indicated are the 4000 Å break (D4000), the emission lines OI, OII and OIII, and the stellar absorption features Fe4668 Å, the G-band at 4300 Å (G4300), Mgb at 5170 Å, and NaD at 5900 Å. (right) Confidence contours for the fit of the Worthey (1994) models to the stellar absorption lines for a range of ages and metallicities. The absorption line strengths are compatible with high metallicity ( $[\text{Fe}/\text{H}] > 0.2$ ) old ( $> 9$  Gyr) stellar populations.

colours, because the range of absorption features can be used to disentangle age and metallicity effects (Worthey 1994). Furthermore, the measured equivalent widths of the lines are less influenced by calibration errors. The three highest signal-to-noise spectra of the most nearby GPS galaxies were shifted to the rest-frame and combined together to form a composite GPS galaxy spectrum (figure 2). The spectrum clearly shows the 4000 Å break and several deep stellar absorption lines, with as most prominent, the G-band at 4300 Å, Fe4668 Å, MgB at 5175 Å and NaD at 5900 Å, with equivalent widths of 6.7, 7.3, 5.0 and 4.5 Å respectively. The absorption line indices were compared with the Worthey (1994) models to estimate their age and metallicity. According to these models, the dominant light of these galaxies is coming from a stellar population with an age > 9 Gyr and a metallicity between 1.5 and 2.5 times solar (figure 2).

Optically selected ellipticals show a strong correlation between absorption line strengths and mass (Dressler et al. 1987): the more massive the galaxy, the deeper the absorption lines. This indicates that giant ellipticals are more metal rich and/or have older stellar populations than smaller ellipticals. The deep stellar absorption lines in the GPS galaxies are therefore consistent with them being among the most massive ellipticals, as found by Snellen et al. (1996a, 1996b). This makes it unlikely that a non-stellar contribution from the active nucleus is present in the optical continuum of these galaxies. Even a small contribution of, say 5%, would make the intrinsic absorption lines 5% deeper, resulting in even higher ( $\sim 20\%$ ) metallicities and/or ages, which would correspond to unlikely ages higher than the age of the universe, and masses larger than those for central cluster galaxies. The claim that GPS galaxies are ideal objects to study the cosmological evolution of giant ellipticals seems therefore justified.

## 4.2 The Optical Spectra of GPS Quasars

In optical studies of quasars, GPS sources are generally treated as flat-spectrum radio sources. It is interesting to compare the optical (restframe UV) spectra of GPS quasars with those of the general population of flat-spectrum quasars, to see whether a distinction can be made between the two classes of objects. Any differences may provide important evidence on the influence Doppler boosting and orientation have on the optical and radio spectra of GPS quasars.

### 4.2.1 The composite GPS quasar spectrum

Baker and Hunstead (1995) have studied a sample of flat spectrum quasars as a function of their ratio of radio core-to-lobe flux density to reveal the effects of orientation. They divided the quasars in their sample into three sub-samples according to their radio core-to-lobe ratios  $R$ ;  $R > 1$  (core dominated),  $0.1 < R < 1$  (intermediate), and  $R < 0.1$  (lobe dominated). They found that core-dominated quasars have bluer optical spectra, a stronger 3000 Å bump and smaller equivalent widths than lobe dominated quasars. All these trends can be accounted for assuming an increase in dust extinction with viewing angle. In addition, Baker and Hunstead (1995) found the spectra of CSS quasars to have evidence of even more reddening, with steep powerlaw continua,

strong low-ionisation narrow-line emission, and no 3000 Å bump.

Following the same procedure as Baker and Hunstead (1995) we produced a composite GPS quasar spectrum. To derive the composite spectrum, each individual spectrum was shifted to the quasar rest frame, and fitted with a power-law,  $F(\nu) \propto \nu^k$ , in the wavelength ranges 1300 – 1500, 1700 – 1850, and 1950 – 2200 Å, thereby avoiding the influence of emission lines and contamination by the 3000 Å bump. This power law fit was used to find the level of the continuum at 3000 Å and to normalise the spectra at this wavelength. The redshifted and normalised spectra were then co-added without using any weighting. Because of obvious flux calibration problems, the data from the red ISIS arm of B0601+5753 and B0758+5929, and the data blueward of 4500 Å of B0758+5929 and B0826+7045, could not be used in this process.

By normalising the spectra at a given wavelength, spectral slope characteristics have largely been preserved. However, to be able to make a comparison with the Baker and Hunstead results, the spectra have been normalised at the same wavelength (3000 Å), which for all our quasars is at or even beyond the red end of their observed spectrum. This makes the contribution of the blue quasars stronger than the red quasars in the composite spectrum, but this effect should be similar in the Baker and Hunstead results in this part of the spectrum. The composite spectrum is shown in figure 3. Below 1500 Å the composite spectrum is very inaccurate, because only a few quasars, the ones with the highest redshifts, contribute to this part of the spectrum. The fitted power law, indicated by the dashed line, has a spectral index of 0.8, using the wavelength ranges 1300 – 1500, 1700 – 1850, and 1950 – 2200 Å. However, when using only the wavelength ranges 1700 – 1850, and 1950 – 2200 Å, a spectral index of 0.7 is obtained, indicating the uncertainty in the fit caused by the spectral curvature. Even taking into account this uncertainty the 3000 Å bump is clearly visible. The equivalent widths of Ly $\alpha$ , CIV, CIII] and MgII are 65 Å, 25 Å, 20 Å and 25 Å, respectively.

The composite GPS quasar spectrum is clearly different from that of CSS quasars and is similar to that constructed for flat-spectrum quasars (Baker and Hunstead, 1995). The spectral slope measured for the composite GPS quasar spectrum is comparable to that for the intermediate sub-sample (0.7), and the strength of the 3000 Å bump is consistent with both the core-dominated and intermediate sub-sample. The equivalent widths of the major emission lines matches better those of the core-dominated quasars (Ly $\alpha$  = 70 Å, CIV = 50 Å, CIII] = 34 Å and MgII = 43 Å) than those of the lobe-dominated quasars (CIV = 120 Å, CIII] = 16 Å and MgII = 71 Å). The composite GPS quasar spectrum shows that the average optical properties of GPS quasars are indistinguishable from those of flat-spectrum quasars in general, but that they appear to be more like core-dominated quasars than lobe-dominated quasars. It is likely that GPS quasars are also present in the Baker and Hunstead (1995) sample. They will appear in the core-dominated sub-sample because the  $R$  values are measured at  $\sim 1''$  resolution. The composite GPS quasar spectrum is therefore consistent with the Baker and Hunstead result. Note however that the redshift distribution for the GPS quasars is different from that of flat-spectrum quasars and that of CSS quasars. For the

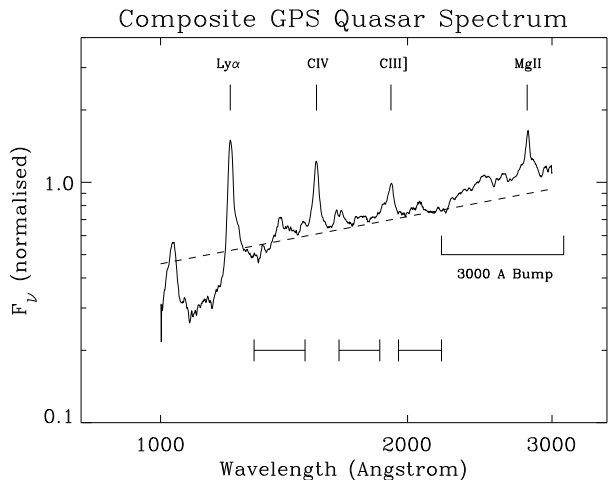


**Figure 3.** A composite spectrum of the GPS quasars in our sample for which we have obtained spectra. The dashed line indicates the fit to the continuum between 1300 and 2200 Å. Redward of 2300 Å the 3000 Å bump is visible. The composite spectrum is similar to that of flat spectrum quasars (Baker and Hunstead 1995) and more like core-dominated than lobe-dominated quasars, but clearly different from that of CSS quasars.

samples used, GPS quasars are biased towards the highest redshifts and CSS quasars are biased towards the lowest redshifts, and within the sample of flat-spectrum quasars, the core-dominated quasars are biased towards higher redshifts than the lobe-dominated quasars. The cosmological evolution of dust in the vicinity of quasars may therefore influence this result, and any conclusions must be drawn with caution. The evidence for a low dust extinction in GPS quasars may indeed indicate a small viewing angle as proposed by Baker and Hunstead for core-dominated quasars, but it can also reflect a decrease in dust-content with redshift.

#### 4.2.2 The Baldwin effect in GPS quasars

A major effect in quasar spectra is the Baldwin effect, in which the equivalent width of the CIV  $\lambda 1549$  line decreases with increasing continuum luminosity, particularly in quasars that are flat spectrum radio sources (Baldwin 1977, Baldwin, Wampler and Gaskell 1989). In photo-ionisation models for quasars, the line luminosity is linearly dependent on the continuum luminosity, but is also a strong function of the density and ionisation parameters. The Baldwin effect is believed to be a consequence of an ionisation parameter decreasing with luminosity (Mushotzky and Ferland, 1984). Interestingly, due to the fact that the line flux is not Doppler boosted, the scatter in the CIV-continuum luminosity relation can be used to put an upper limit on the average Doppler factors for the optical continuum in GPS quasars (Kinney et al. 1985).

To investigate the Baldwin effect in GPS quasars, our sample has been complemented with objects from the complete sample of radio-bright GPS sources of Stanghellini et al. (1998). This results in an additional 5 GPS quasars at  $z > 1.9$  with their CIV emission-line subsequently redshifted to optical wavelengths. The CIV emission line properties of these radio-bright GPS quasars are taken from the literature

and shown in table 3. The Baldwin effect for the 17 GPS quasars is shown in figure 4. The spectra of 3 quasars show clear evidence that their CIV emission lines are severely disrupted by associated absorption, which greatly decreases their line luminosities and equivalent widths. These objects, B0554+5847, B0758+5929, and B1746+6921, are indicated by open squares in figure 4. The spectrum of quasar B1945+6024 is of insufficient signal-to-noise to determine whether CIV absorption is present. However, the low equivalent width with respect to the continuum luminosity indicates that CIV absorption is indeed important. Although evidence of the Baldwin effect for the remaining quasars is mainly based on the one low luminosity source, its strength and scatter is comparable to that for flat spectrum quasars (dotted line, Baldwin, Wampler and Gaskell, 1989). The continuum luminosity at 1549 Å is plotted against the CIV line luminosity in figure 5, with the solid line indicating the best fit. A linear relation between the two quantities is indicated by the dotted line, and the difference between this linear relation and the observed relation is an alternative way of plotting the Baldwin effect.

The scatter in the CIV - continuum luminosity relation is only 30%. Although in general GPS quasar spectra show evidence for low dust contents, the scatter may be partially induced by the ratio of dust extinction towards the CIV and continuum emission regions changing from quasar to quasar. More interestingly, the fact that the CIV emission line is emitted isotropically (and not too much affected by dust at small viewing angles to the line of sight) allows the scatter to be used to put an upper limit on the optical Doppler boosting. For example, if the optical continuum is Doppler boosted, the emission line luminosity is independent of viewing angle (disregarding extinction), but the continuum luminosity is a strong function of viewing angle. Therefore a sample of quasars with viewing angles randomly distributed within a certain range will result in a larger scatter in the CIV - continuum luminosity relation. A population of quasars with randomly distributed viewing angles within  $45^\circ$  and with velocities of  $\beta = v/c = 0.5$  have optical continua which are on average Doppler boosted by a factor 5, and produce a 30% scatter in the CIV - continuum luminosity relation. If a smaller quasar opening angle is used, the scatter is lower due to a smaller range in viewing angles. However, if the quasar-opening-angle is reduced in such a way that the scatter allows  $\beta = 0.9$ , quasar-to-quasar variations in  $\beta$  are likely to produce a much larger scatter in the observed CIV-continuum luminosity relation. The low scatter in the Baldwin effect therefore indicates that the optical emission of GPS quasars is only mildly Doppler boosted, unless there is only a small range in both  $\beta$ s and viewing angles.

A weak correlation between the CIV luminosity and radio luminosity (figure 6) enables us to perform a similar analysis on the radio emission. Assuming that the factor 3 scatter is produced by source to source variations in Doppler boosting leads to an upper limit of  $\beta < 0.85$  and the conclusion that the dominant radio emission in GPS quasars is on average not more Doppler boosted than by a factor of 15.

Source	$z$	$S_{cont}$ ( $\frac{erg}{cm^2 s \text{ \AA}}$ )	$L_{CIV}$ ( $\frac{erg}{cm^2 s}$ )	W(CIV) ( $\text{\AA}$ )	Ref.
0237-233	2.223	1.2e-15	1.5e-13	39	1,2
0457+024	2.384	6.9e-17	1.1e-14	45	3
1442+101	3.544	2.3e-16	1.4e-14	14	4
2126-158	3.270	6.0e-16	3.6e-14	14	4
2134+004	1.936	5.4e-16	5.2e-14	33	3

References:

1: Wills et al. 1993

2: Wilkes et al. 1983

3: Baldwin, Wampler and Gaskell, 1989

4: Osmer, Porter and Green, 1994

**Table 3.** The GPS quasars from the radio-bright GPS sample of Stanghellini et al. (1998) with measured CIV  $\lambda 1549 \text{ \AA}$  emission line properties. Column 1 gives the name, column 2 the redshift, column 3 the continuum luminosity at  $1500 \text{ \AA}$ , column 4 the line luminosity, column 5 the restframe equivalent width, and column 6 the references.

### 4.3 The Redshift Distributions of GPS Galaxies and Quasars

The optical counterparts of GPS sources at redshifts smaller than unity are seldomly found to have broad emission lines (eg. Stanghellini et al. 1998). For some of those, the contrast between the stellar and non-stellar emission is low (eg. 1404+286; Osterbrock and Cohen, 1979 and B1622+6630; this paper) which is why they are called Broad Line Radio Galaxies (BLRG) instead of quasars. Other ‘low’ redshift GPS sources also have a substantial non-stellar contribution in their optical light as indicated by a power-law optical spectrum but have no broad emission lines (eg. 2342+821 (Lawrence et al., 1996) and 0531+6121; this paper). However the large majority of low redshift GPS sources ( $\sim > 75\%$ ) are galaxies which show, apart from some narrow emission lines, no evidence for a contribution of non-thermal emission in the optical. High redshift GPS sources ( $z > 1.5$ ) are generally found to be genuine quasars (O’Dea 1990, O’Dea et al. 1991) with strong broad emission lines and no sign of the underlying host galaxies due to the high contrast between non-thermal nuclear emission and integrated star light.

It is important to establish whether this dependence of optical host with redshift is genuine, or whether it is due to selection effects; i) The known redshifts of GPS galaxies are likely to be biased towards low redshift because it is increasingly difficult to measure their emission line features with redshift (at least up to  $z \sim 2$  at which Ly $\alpha$  and CIV are shifted into the optical band). Note that the small fraction of low redshift BLRGs would be identified as galaxies if located at high redshift, since their  $H_\alpha/H_\beta$  ratio and stellar absorption lines indicate that the non-stellar component is strongly absorbed and not visible at rest-frame UV wavelengths. Therefore, the classification of BLRG as galaxies and not as quasars does not bias the redshift distributions. ii) The high redshift GPS quasars are found to have substantially higher rest-frame radio peak frequencies than the GPS galaxies (Stanghellini et al. 1998, Snellen et al. 1998b). If a population of low redshift GPS quasars with similar peak frequencies as the high redshift quasars exists, it would not

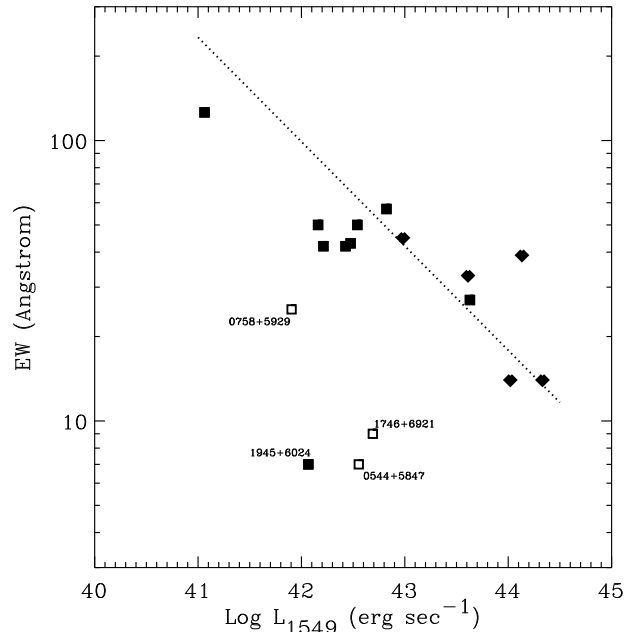


**Figure 4.** The CIV Baldwin effect for GPS quasars. The squares indicate objects from the faint WENSS sample and the diamond symbols quasars from the Stanghellini et al. (1998) sample. The open squares indicate quasars which show clear evidence for associated CIV absorption, which significantly reduces the observed CIV equivalent widths for these objects. The quasar B1945+6024 is possibly affected by absorption as well, but the spectrum is of too low signal to noise to confirm this. The dotted line shows the strength of the Baldwin effect in flat spectrum quasars from Baldwin, Wampler and Gaskell (1989).

have been included in the radio-bright samples due to their too high *observed* radio-peak frequencies.

Both selection effects can be investigated with our faint sample. Due to the well established Hubble diagram for GPS galaxies (Snellen et al. 1996a), the redshifts of the GPS galaxies can be estimated using their optical  $R$  band magnitude. Although this method results in an increasing uncertainty with redshift, we believe it is sufficient to establish differences between the redshift distributions. The faint GPS sample has been constructed in such a way that if an object falls within the sample at  $z = z_{gps}$ , it also would have been in the sample if it was located at  $z < z_{gps}$ . This is due to the fact that the sources are selected on the optically thick (inverted) part of their radio spectrum, and no high-frequency cut-off has been made. The shift in the peak frequency to higher values due to a lower redshift would be compensated for by an increase in the peak flux density. For example, the GPS quasar B1945+6024 at  $z=2.70$  is in our sample, although it has an (undetermined) peak frequency larger than 15 GHz. No low redshift GPS quasars are found in our sample, which makes it unlikely that a significant population of low redshift GPS quasars is missing in the current GPS samples.

Knowing it to be free from major selection effects, the redshift distributions of the quasars and galaxies in the complete radio-bright GPS sample of Stanghellini et al (1998) and the faint sample can be compared. The radio luminosities

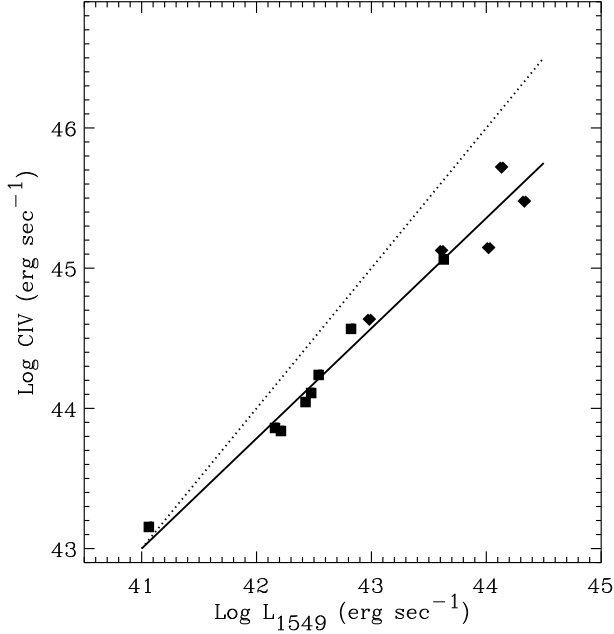


**Figure 5.** The continuum luminosity at 1549 Å versus the CIV line luminosity for GPS quasars, excluding the ones influenced by associated absorption. The deviation from a linear correlation, indicated by the dotted line, is an alternative way of showing the Baldwin effect. The low dispersion in the relation between the isotropic CIV line luminosity and the continuum luminosity indicates that the continuum emission can only be mildly Doppler boosted.

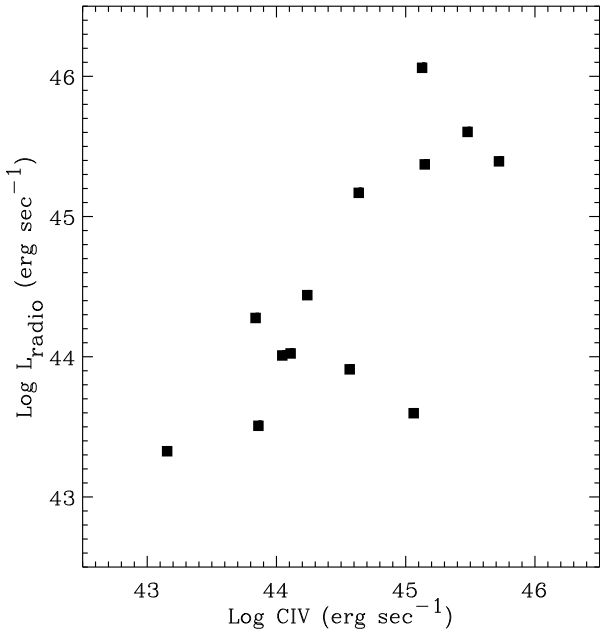


**Figure 6.** The isotropic CIV line luminosity versus the radio luminosity. Although the scatter is large in this correlation, it provides an upper limit to the effect of Doppler boosting on the dominant radio components in GPS quasars.

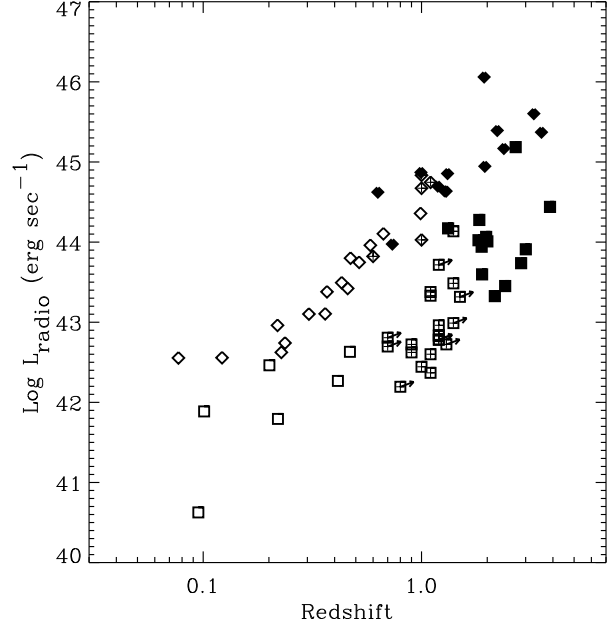


**Figure 7.** The redshift versus radio luminosity for the GPS sources in the radio-bright sample of Stanghellini et al (1998, diamonds) and our radio-faint sample (squares). The open symbols indicate galaxies, and the filled symbols quasars. The crossed squares are galaxies with redshifts estimated from their optical apparent.

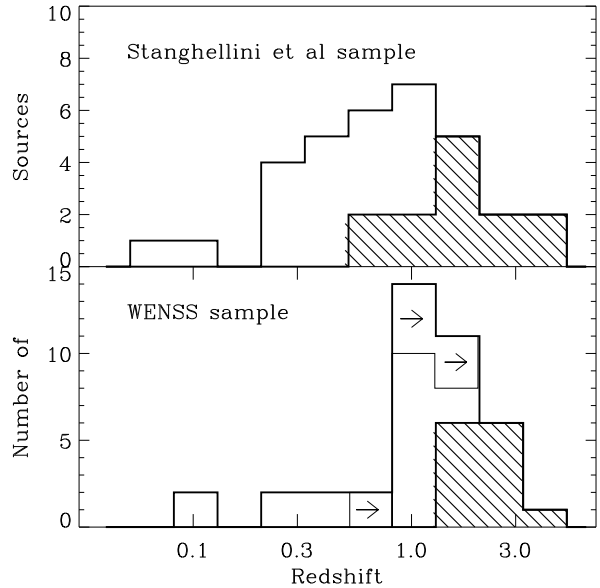


**Figure 8.** The redshift distributions of the GPS galaxies (open) and quasars (filled) in the radio-bright sample of Stanghellini et al. (upper panel) and the radio-faint sample (bottom panel). Note that there is a large uncertainty in the redshift distribution of the radio-faint galaxies.

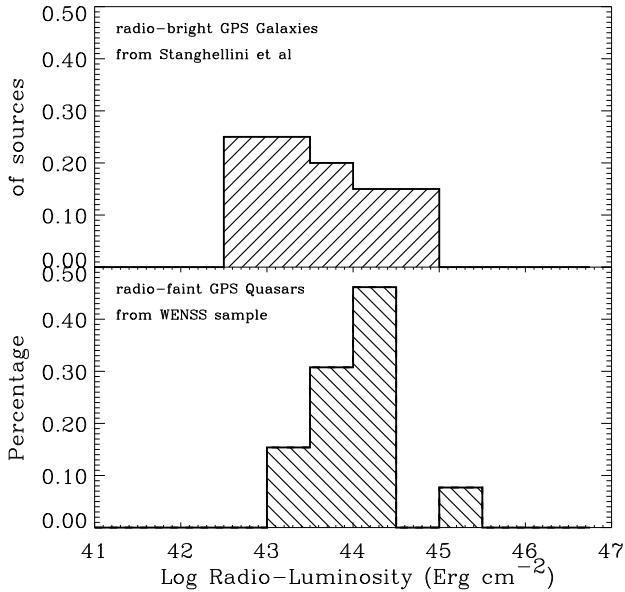


**Figure 9.** The radio luminosities of the GPS galaxies in the radio-bright sample are comparable to those of the GPS quasars in the radio-faint sample.

ties of the objects in both samples are calculated as the peak frequency times the peak flux density, and assuming  $H_0 = 50$  km/sec/Mpc and  $q_0 = 0.5$ . For only five (25%) of the GPS galaxies in the Stanghellini et al. sample the redshifts were to be estimated from their  $R$  band magnitudes. This method had to be used for the majority of the galaxies in the faint sample (80%), and for 8 of these (26%) only a lower limit of the redshift could be obtained. All the redshifts of the quasars in the bright sample and 70% of those in the faint sample have been measured. The radio luminosities of the GPS sources versus redshift are shown in figure 7. The diamonds indicate sources from the bright sample and the squares indicate sources from the faint sample. Filled symbols are quasars and open symbols are galaxies. Clearly in both samples the galaxies are found at low redshift and the quasars at high redshift. The GPS galaxies in the faint sample are biased towards higher redshift than the galaxies in the radio-bright sample (figure 8). In the faint sample, only 6 out of 27 galaxies (22%) are found at  $z \leq 0.5$ , while in the radio-bright sample 12 out of 19 galaxies (63%) are found at  $z \leq 0.5$ . In addition, the faintest galaxies in the radio-faint sample are fainter than the faintest galaxies in the radio-bright sample. However, at present, it is not clear whether this is due to lower optical luminosities or higher redshifts of the host galaxies. A small fraction of the faint and red optical identifications may turn out to be quasars instead of galaxies. However, if quasars, they are most likely to be at even higher redshifts than the optically brighter quasars, since the colours of quasars at  $z > 2$  become rapidly redder with redshift due to the absorption by intervening Ly $\alpha$  (eg. Hook et al., 1995). Therefore, this would unlikely affect the observed difference in redshift distribution.

The fact that in both samples the galaxies are found

at low redshift and the quasars at high redshift, indicates that these different redshift-distributions are not caused by a radio-power effect; the higher the radio power, the larger the chance to see the quasar nucleus. Such an effect, that may be caused by a luminosity-dependent quasar opening-angle, could in a flux density limited sample lead to the dependence of optical host with redshift. However, finding a similar effect in both the faint and bright sample rules out this possibility. In figure 9 it is shown that the radio-luminosities of the GPS galaxies in the radio-bright sample are comparable to the luminosities of the GPS quasars in the radio-faint sample. This, combined with the fact that the quasar fraction is the same in both samples within the uncertainties, indicates that the galaxy-quasar difference is not a radio-power effect but a redshift effect.

The lifetime of a radio source is much smaller than cosmological time scales. Therefore, if GPS quasars and galaxies are unified by orientation, their different redshift distributions imply that the quasar opening angle is a strong function of redshift. However, such a strong dependence of opening angle with redshift needed to explain the data is not found for other types of radio-loud AGN. Snellen et al. (1998c) show that if GPS galaxies were oriented towards us, that their overall radio spectrum would change from gigahertz peaked to flat spectrum and variable, due to Doppler boosting of the inner radio components. This is a strong indication that GPS galaxies and quasars are not unified by orientation and that they form two distinct classes of objects which just happen to have the same observed radio-spectral properties.

In this case, the GPS quasars may be a sub-class of flat spectrum sources in general, having physical parameters at one end of the range seen in flat spectrum quasars. A model should account for their low flux density variability, peaked radio spectra, low extinction optical spectra, and low dispersion in the CIV-continuum relation as presented in section 4.2.2. For example, the GPS quasars may have slower jets (due to a denser medium, O’Dea et al. 1991) than the flat spectrum quasars in general, or their jets may be pointed more towards us resulting in a larger optical depth and possible synchrotron self absorption. A detailed comparison of the redshift distributions and the radio-spectral properties of GPS and flat spectrum quasars, including variability studies, are needed to further investigate this hypothesis.

## 5 CONCLUSIONS

We have presented spectroscopic observations of a sample of faint Gigahertz Peaked Spectrum (GPS) radio sources drawn from the Westerbork Northern Sky Survey (WENSS). Redshifts have been determined for 19 (40%) of the objects. The optical spectra of the low redshift GPS galaxies show deep stellar absorption features, which confirms that their optical light is not significantly contaminated by AGN-related emission, but is dominated by a population of old (>9 Gyr) and metal-rich (>0.2 [Fe/H]) stars. The optical spectra of GPS sources identified with quasars are indistinguishable from those of flat spectrum quasars. Their blue colours and strong 3000 Å bump indicate low dust extinction, which is comparable to the spectra of core-dominated quasars, but clearly different from the spectra of Compact

Steep Spectrum (CSS) quasars. The low dispersion in the Baldwin effect for GPS quasars indicates that their optical continuum can only be mildly Doppler boosted. The redshifts of the GPS quasars in our radio-faint sample are comparable to those in the bright samples presented in the literature, and are preferentially found at  $z \sim 2 - 3$ . The construction of the radio-faint sample was such, that it is unlikely that a significant population of low redshift GPS quasars has been missed due to selection effects. We therefore claim that there is a genuine difference between the redshift distributions of GPS galaxies and quasars which, because it is present in both the radio-faint and bright samples, can not be due to a redshift-luminosity degeneracy. It is unlikely that the GPS quasars and galaxies are unified by orientation, unless the quasar opening angle is a strong function of redshift. We suggest that the GPS quasars and galaxies are not related and just happen to have identical observed radio-spectral properties, and hypothesise that GPS quasars are a sub-class of flat spectrum quasars in general.

## ACKNOWLEDGEMENTS

We thank the *Comite Cientifico Internacional* (CCI) of the IAC for the allocation of observing time. The Isaac Newton Telescope, and the William Herschel Telescope are operated on the island of La Palma by the Isaac Newton Group in the Spanish Observatorio del Roque de los Muchachos of the Instituto de Astrofisica de Canarias. We thank Richard McMahon and Neal Jackson for taking some of the spectra. This work was in part funded through an NWO programme subsidy and by the European Commission under contracts SCI\*-CT91-0718 (The Most Distant Galaxies) and ERBFMRX-CT96-086 (Formation and Evolution of Galaxies), and ERBFMRX-CT96-0034 (CERES).

## REFERENCES

- Baker J.C. and Hunstead R.W., 1995, *Astrophys. J.*, L95  
 Baldwin J.A., 1977, *Astrophys. J.*, **214**, 769  
 Baldwin J.A., Wampler E.J. and Gaskell C.M., 1989, *Astrophys. J.*, **338**, 630  
 Dressler A., Lynden-bell D., Burstein D., Davies R.L., Faber S.M., Terlevich, R., Wegner G., 1987, *Astrophys. J.*, **313**, 42  
 Fanti R., Fanti C., Schilizzi R.T., Spencer R.E., Nan Rendong, Parma P., Van Breugel W.J.M., Venturi T., 1990, *Astron. Astrophys.*, **231**, 333  
 Fanti C., Fanti R., Dallacasa D., Schilizzi R.T., Spencer R.E., Stanghellini C., 1995, *Astr. & Astrophys.*, **302**, 317  
 Hook I.M., McMahon R.G., Patnaik A.R., Browne I.W.A., Wilkinson P.N., Irwin M.J., Hazard C., 1995, *Mon. Not. R. Astr. Soc.*, **273**, L63  
 Mushotzky R. and Ferland G.J., 1984, *Astrophys. J.*, **278**, 558  
 Kinney A.L., Huggins P.J., Bregman J.N., Glassgold A.E., 1985, *Astrophys. J.*, **291**, 135  
 Lawrence C.R., Zucker J.R., Readhead A.C.S., Unwin S.C., Pearson T.J., Xu W., 1996, *Astrophys. J. Suppl.*, **107**, 541  
 O'Dea C.P., 1990, *Mon. Not. R. Astr. Soc.*, **245**, 20  
 O'Dea C.P., Baum S.A., Stanghellini C., 1991, *Astrophys. J.*, **380**, 66  
 O'Dea C.P., Stanghellini C., Baum S.A., Charlot S., 1996, *Astrophys. J.*, **470**, 806  
 O'Dea C.P., Baum S.A., 1997, *Astron. J.*, **113**, 148  
 O'Dea C.P., 1998, *P.A.S.P.*, **110**, 493  
 Osmer P.S., Porter A.C., Green R.F., 1994, *Astrophys. J.*, **436**, 678  
 Osterbrock and Cohen, 1979, *Mon. Not. R. Astr. Soc.*, **187**, 61  
 Owsianik I. and Conway J., 1998, *Astr. & Astrophys.*, **337**, 69  
 Readhead A.C.S., Taylor G.B., Xu W., Pearson T.J., Wilkinson P.N., Polatidis A.G., 1996, *Astrophys. J.*, **460**, 612  
 Rengelink R.B., Tang Y., de Bruyn A.G., Miley G.K., Bremer M.N., Röttgering H.J.A., Bremer M.A.R., 1997, *Astron. Astrophys. Suppl.*, **124**, 259  
 Snellen I.A.G., Bremer M.N., Schilizzi R.T., Miley G.K., van Ojik R., 1996a, *Mon. Not. R. Astr. Soc.*, **279**, 1294  
 Snellen I.A.G., Bremer M.N., Schilizzi R.T., Miley G.K., 1996b, *Mon. Not. R. Astr. Soc.*, **283**, 123  
 Snellen I.A.G., *PhD thesis* 1997, Leiden Observatory  
 Snellen I.A.G., Schilizzi R.T., de Bruyn A.G., Miley G.K., Rengelink R.B., Röttgering H.J.A., Bremer, M.N., 1998a, *Astr. & Astrophys. Suppl.*, **131**, 435  
 Snellen I.A.G., Schilizzi R.T., Bremer M.N., de Bruyn A.G., Miley G.K., Röttgering H.J.A., McMahon R.G., Pérez Fournon I., 1998b, *Mon. Not. R. Astr. Soc.*, **301**, 985  
 Snellen I.A.G., Schilizzi R.T., de Bruyn A.G., Miley G.K., 1998c, *Astr. & Astrophys.*, 333, 70  
 Stanghellini C., O'Dea C.P., Baum S.A., Dallacasa D., Fanti R., Fanti C., 1997, *Astron. & Astrophys.*, **325**, 943  
 Stanghellini C., O'Dea, C. P., Dallacasa, D., Baum, S.A., Fanti, R., Fanti, C., 1998, *Astron. & Astrophys. Suppl.*, **131**, 303  
 De Vries W.H., Barthel P.D., O'Dea C.P., 1997, *Astronomy and Astrophysics*, **321**, 105  
 Wilkes B.J., Wright A.E., Jauncey D.L., Peterson B.A., 1983, *Proceedings Astr. Soc. of Australia*, **Vol. 5**, no. 1, p2  
 Wills B.J., Netzer H., Brotherton M.S., Han Mingsheng, Wills D., Baldwin J.A., Ferland G.J., Browne I.W.A., 1993, *Astrophys. J.*, **410**, 534  
 Worthey G., 1994, *Astrophys. J. Suppl.*, **95**, 107